COMPUTATIONS OF NEEDLE-LIKE MICROSTRUCTURES

ZHIPING LI

SCHOOL OF MATHEMATICAL SCIENCES, PEKING UNIVERSITY,
BEIJING 100871, P.R. CHINA

Abstract. We report some numerical results on the computation of needle-like microstructrues at mesoscopic scale obtained by applying the mesh transformation method, which basically includes a mesh optimization into the finite element approximations, on a nonquasiconvex elastic crystal model. Numerical experiments show that the branched needle-like microstructures can be well resolved near the interfaces between twinned layers of martensite and a single variant of martensite, which are in good qualitative agreement with the physical experiments.

1. Introduction

Crystalline microstructure is a typical phenomenon commonly found in solid crystal materials. A geometrically nonlinear theory [1, 2] models the phenomenon by a problem of minimizing a potential energy

$$F(u;\ \Omega) = \int_\Omega f(\nabla u(x))\, dx \tag{1.1}$$

with a nonquasiconvex energy density $f : R^{mn} \to R^1$ on a set of admissible functions

$$\mathbb{U}(u_0;\ \Omega) = \{u \in W^{1,p}(\Omega; R^m) : u = u_0,\ \text{on } \partial\Omega_0\}, \tag{1.2}$$

where $\Omega \subset R^n$ is a bounded open set with a Lipschitz continuous boundary $\partial\Omega$, $\partial\Omega_0$ is a subset of $\partial\Omega$ with positive $(n-1)$-dimensional measure and $1 < p < \infty$.

It is well known that such a variational problem fails, in general, to have a solution, and the minimizing sequences of the potential energy can develop finer

---

1991 *Mathematics Subject Classification.* 73C50, 65K10, 65N12, 65N30.

Key words and phrases. nonquasiconvex, mesh transformation, twinned layers, branch, needle-like microstructure, interface, metastable state.

The research was supported in part by the Special Funds for Major State Basic Research Projects (G1999032802), NSFC and RFDP of China.

and finer oscillations and lead to microstructures [1, 2], which are characterized by the gradient Young measure [3]. To compute the microstructures, or rather the highly oscillating minimizing sequences of $F(\cdot,\ \Omega)$ in $\mathbb{U}(u_0;\ \Omega)$, is challenging and is of great interests both in theory and in applications. Great progress has been made in recent years, and many numerical methods have been established (see among many others [4]-[23]). Numerical analyses and experiments revealed that the numerical results often depend strongly on the mesh and shape functions, and can sometimes lead to pseudo-microstructures [7, 11, 14]. A rotational transformation method established by Li [15] and the discontinuous finite element method established by Gobbert and Prohl [17] somehow reduce the mesh dependence of the numerical results. The rotational transformation method is recently further developed into a mesh transformation method [18] and a periodic relaxation method [19] which turn out to be very successful in computing macroscopic information, *i.e.* the gradient Young measure, of the twinned laminated microstructures.

While the periodic relaxation method is efficient in computing twinned laminates at macroscopic scale, it is not designed to capture the mesoscopic phenomenon of microstructures, for example the needle-like microstructure near the interfaces between twinned layers and single variant of martensite [22]-[26]. However we shall see in the present paper that the idea of the mesh transformation method (see [18, 19]) can be applied for such a purpose. Basically, the advantage of the mesh transformation method is that it allows the mesh to be aligned with the interfaces during the process of optimization, so that a sharper numerical approximation can be made and a much relaxed discrete optimization problem is produced.

In section 2, we shall introduce the mesh transformation method and prove its convergence. In section 3, some numerical results, which are obtained by applying the mesh transformation method to a two-dimensional model for elastic crystals and using the conjugate gradient method to solve the resulted discrete optimization problem, are presented to show the efficiency of the method in computing at the mesoscopic scale the needle-like microstructures and their bending and branching near the interfaces between the twinned layers of martensite and single variant of martensite, which are in good qualitative agreement with the experiment of Chu and James [24, 27].

It is worth noticing that, instead of resulting from the balance of the elastic energy and the surface energy across twin boundaries as in [28], or a fixed length scale of twinned layers in the boundary data as in [23], our computation shows that initially existing twinned layers can also branch and produce needle-like microstructures as the initially existing twinned layers approach the interfaces of laminate-single variant of martensite. Of course, what the method produces are local minimizers or metastable states of the elastic energy. Numerical evidence shows that there can be many stable local minimizers or metastable states which have bending and branching needles.

2. The mesh transformation method

Let $\Omega \subset R^n$ be a polyhedron and let $\partial\Omega$ be its boundary. Let $\partial\Omega_0$ be a subset of $\partial\Omega$ with positive $(n-1)$-dimensional measure. Let $f : R^{mn} \to R^1$ be a continuous function which satisfies the following hypotheses for a constant $p > 1$:

(h1): $\max\{0, a_1 + b_1|\xi|^p\} \le f(\xi) \le a_2 + b_2|\xi|^p$,
(h2): $|f(\xi) - f(\eta)| \le C(1 + |\xi|^{p-1} + |\eta|^{p-1})|\xi - \eta|$,

where $a_1 \in R^1$, $a_2 > 0$, $b_2 \ge b_1 > 0$ and $C > 0$ are constants. Consider the problem of minimizing the functional

$$F(u;\ \Omega) = \int_\Omega f(\nabla u(x))\, dx \tag{2.1}$$

on a set of admissible functions

$$\mathbb{U}(u_0; \Omega) = \{u \in W^{1,p}(\Omega; R^m) : u(x) = u_0(x),\ \text{on } \partial\Omega_0\}, \tag{2.2}$$

where u_0 is a given Lipschitz continuous boundary data.

Define

$$T(\Omega) = \{\text{bijections } L : \bar\Omega \to \bar\Omega | L \in W^{1,\infty}(\Omega;\ R^n), L^{-1} \in W^{1,\infty}(\Omega;\ R^n),$$
$$L(\partial\Omega_0) = \partial\Omega_0,\ \text{and } \det \nabla L > 0, a.e. \text{ in } \Omega\}.$$

For any $L \in T(\Omega)$ and $u \in \mathbb{U}(u_0; \Omega)$, let $A \in R^{mn}$ and let $\bar u(x) : \Omega \to R^m$ be defined by

$$\bar u(x) = u(L(x)) - A\, L(x). \tag{2.3}$$

Then it is easily seen that $\bar u \in \mathbb{U}(\bar u_0; \Omega)$, where $\bar u_0(x) = u_0(L(x)) - A\, L(x)$,

$$\int_\Omega f(A + \nabla \bar u(x)(\nabla L(x))^{-1}) \det \nabla L(x)\, dx = F(u;\ \Omega), \tag{2.4}$$

and

$$\inf_{\bar{u}\in\mathbb{U}(\bar{u}_0;\Omega)} F(\bar{u}, L;\ \Omega) = \inf_{u\in\mathbb{U}(u_0;\Omega)} F(u;\ \Omega), \tag{2.5}$$

where

$$F(\bar{u}, L;\ \Omega) = \int_\Omega f(A + \nabla\bar{u}(x)(\nabla L(x))^{-1}))\det\nabla L(x)\,dx. \tag{2.6}$$

Let $\mathfrak{T}_h(\Omega)$ be regular triangulations of Ω with mesh sizes h [31]. Let

$$T_h(\Omega) = \{L \in T(\Omega) : L|_K \text{ is affine } \forall K \in \mathfrak{T}_h(\Omega)\}, \tag{2.7}$$

$$\mathbb{U}_h(\Omega) = \{u \in C(\overline{\Omega};\ R^m) : u|_K \text{ is affine } \forall K \in \mathfrak{T}_h(\Omega)\} \tag{2.8}$$

and

$$\mathbb{U}_h(v;\Omega) = \{u \in \mathbb{U}_h(\Omega) : u|_{\partial\Omega_0} = v\}. \tag{2.9}$$

In the mesh transformation method, we consider the linear boundary condition $u|_{\partial\Omega_0} \equiv u_0 = A\,x$ and solve the following discrete problem:

$$(DP)\quad \begin{cases} \text{find } (u,\ L) \in \mathbb{U}_h(0;\ \Omega)\times T_h(\Omega) \text{ such that} \\ F(u, L;\ \Omega) = \inf_{(u',L')\in\mathbb{U}_h(0;\,\Omega)\times T_h(\Omega)} F(u', L';\ \Omega). \end{cases} \tag{2.10}$$

Theorem 2.1. *Let the sequences $h_i > 0$ and $\varepsilon_i > 0$ satisfy $\lim_{i\to\infty} h_i = 0$ and $\lim_{i\to\infty}\varepsilon_i = 0$. Let the functions $(\bar{u}_{h_i},\ L_{h_i}) \in \mathbb{U}_{h_i}(0;\ \Omega)\times T_{h_i}(\Omega)$ be a sequence of approximate solutions to (DP) (see remark 2.1) with*

$$F(\bar{u}_{h_i},\ L_{h_i};\ \Omega) \le \inf_{(\bar{u},L)\in\mathbb{U}_{h_i}(0;\,\Omega)\times T_{h_i}(\Omega)} F(\bar{u}, L;\ \Omega) + \varepsilon_i.$$

Then

$$\lim_{i\to\infty} F(u_{h_i},\ L_{h_i}(\Omega)) = \lim_{i\to\infty} F(\bar{u}_{h_i},\ L_{h_i};\ \Omega) = \inf_{u\in\mathbb{U}(u_0;\Omega)} F(u,\ \Omega), \tag{2.11}$$

where $u_{h_i}(x) = \bar{u}_{h_i}(L_{h_i}^{-1}(x)) + A\,x$ and $u_0(x) = A\,x$ for $x \in \partial\Omega_0$ (see (2.3)).

Proof. It follows from (2.5) that

$$\inf_{u\in\mathbb{U}(u_0;\Omega)} F(u;\ \Omega) = \inf_{\bar{u}\in\mathbb{U}(0;\,\Omega)} F(\bar{u}, L_{h_i};\ \Omega) \le F(\bar{u}_{h_i}, L_{h_i};\ \Omega). \tag{2.12}$$

On the other hand, for the identity map $I : \Omega \to \Omega$, we have

$$F(\bar{u}_{h_i}, L_{h_i};\Omega) \le \inf_{\bar{u}\in\mathbb{U}_{h_i}(0;\,\Omega)} F(\bar{u}, I;\ \Omega) + \varepsilon_i. \tag{2.13}$$

Now, let $\{u_i\} \subset W^{1,p}(\Omega;\ R^m)$ be a minimizing sequence of $F(u;\ \Omega)$ in $\mathbb{U}(u_0; \Omega)$. By the continuity of the functional $F(u;\ \Omega)$ in $W^{1,p}(\Omega;\ R^m)$, which is a consequence of the hypothses (h1) and (h2), and the fact that $C^\infty(\Omega;\ R^m) \cap \mathbb{U}(0;\ \Omega)$ is dense in $\mathbb{U}(0;\ \Omega)$ in the strong topology of $W^{1,p}(\Omega;\ R^m)$ [32], without loss of generality it may be assumed that $\{u_i\}$ are smooth functions. By the standard finite element interplation theory [31], we have

$$u_{i,h} \longrightarrow u_i, \text{ in } W^{1,p}(\Omega;\ R^m) \text{ as } h \to 0,$$

where $u_{i,h}$ is the finite element interpolating function of u_i in $\mathbb{U}(u_0; \Omega)$. Thus, by the continuity of the funtional $F(u;\ \Omega)$ in $W^{1,p}(\Omega;\ R^m)$, we have

$$\lim_{h_i \to 0} \inf_{\bar{u} \in \mathbb{U}_{h_i}(0;\ \Omega)} F(\bar{u}, I;\ \Omega) = \inf_{\bar{u} \in \mathbb{U}(0;\ \Omega)} F(\bar{u}, I;\ \Omega) = \inf_{u \in \mathbb{U}(u_0; \Omega)} F(u;\ \Omega). \tag{2.14}$$

This completes the proof. $\square$

Remark 2.1. The minima of (DP) may not be attainable, since the mesh can be so singularly deformed that the measure of some of the elements goes to zero.

Remark 2.2. We may use the conjugate gradient method to search for a minimizer of (DP). Since it is a local method, only local minimizers can be found. In fact, lack of surface energy, what we are most interested in are those most easily formed local minimizers or metastable states of the elastic energy. As in the case of the global convergence given by Theorem 2.1, we can also expect better numerical results by the mesh transformation method for the metastable states or local minimizers, since the method enriches the finite element function spaces and thus can provide a better approximation. We also found in our numerical experiments that allowing the mesh to move greatly improves the convergent speed of the minimizing procedure.

3. Numerical Experiments and Results

In the following numerical examples, we use a modified Ericksen-James two dimensional energy model for elastic crystals with $f(A,\ \theta) = \Phi(A^T A,\ \theta)$ and

$$\Phi(C,\ \theta) = \frac{b(\theta)}{4}(C_{11} - C_{22})^2 - \frac{c(\theta)}{8}(C_{11} - C_{22})^2 |C_{11} - C_{22}| + \frac{d(\theta)}{16}(C_{11} - C_{22})^4 + e\, C_{12}^2 + g(\operatorname{tr} C - 2)^2, \tag{3.1}$$

where

$$
\begin{aligned}
b(\theta) &= (1+\alpha\arctan\mu(\theta-\theta_T))d_0\varepsilon^2,\\
c(\theta) &= 2(1+\frac{1+2\gamma}{3}\alpha\arctan\mu(\theta-\theta_T))d_0\varepsilon,\\
d(\theta) &= (1+\gamma\alpha\arctan\mu(\theta-\theta_T))d_0,
\end{aligned}
$$

and where $d_0>0$, $e>0$ and $g>0$ are the elastic moduli, $0<\varepsilon\ll 1$ is the transformation strain, θ_T is the transformation temperature,

$$
\alpha \approx \frac{2}{\pi},\ \ \mu>0,\ \text{and}\ \gamma<1
$$

are the material constants used to reflect the change of elastic moduli and the energy barriers as the temperature varies.

Figure 1 shows $\Phi(C_\delta,\ \theta)$ as a function of δ with $\alpha=2.02/\pi$, $\mu=0.25$, $\gamma=0$, $\varepsilon=0.05$, $d_0=500$ and $\theta_T=70\,^{\circ}\mathrm{C}$ for various θ, where

$$
C_\delta = \begin{pmatrix} 1+\delta & 0\\ 0 & 1-\delta \end{pmatrix}
$$

It is not difficult to verify (see [29], see also [6, 7, 30]) that the energy density $f(\nabla u,\ \theta)=\Phi((\nabla u)^T\nabla u,\ \theta)$ has

- **(i):** a unique potential well $SO(2)$ for $\theta>\theta_T$;
- **(ii):** two symmetry related rotationally invariant potential wells $SO(2)U_0$ and $SO(2)U_1$ for $\theta<\theta_T$,

where $SO(2)$ is the set of all 2×2 rotational matrices, and

$$
U_0 = \begin{pmatrix} \sqrt{1-\varepsilon} & 0\\ 0 & \sqrt{1+\varepsilon} \end{pmatrix},\quad U_1 = \begin{pmatrix} \sqrt{1+\varepsilon} & 0\\ 0 & \sqrt{1-\varepsilon} \end{pmatrix}. \tag{3.2}
$$

Furthermore, U_0 and $R^{\pm}U_1$ are in rank-one connection. More precisely, let $\eta_1=\sqrt{1-\varepsilon}$ and $\eta_2=\sqrt{1+\varepsilon}$ and let

$$
R^{\pm} = \begin{pmatrix} \eta_1\eta_2 & \pm\varepsilon\\ \mp\varepsilon & \eta_1\eta_2 \end{pmatrix}, \tag{3.3}
$$

then, we have

$$
R^{\pm}U_1 = U_0 + \mathbf{a}^{\pm}\otimes\mathbf{n}^{\pm}, \tag{3.4}
$$

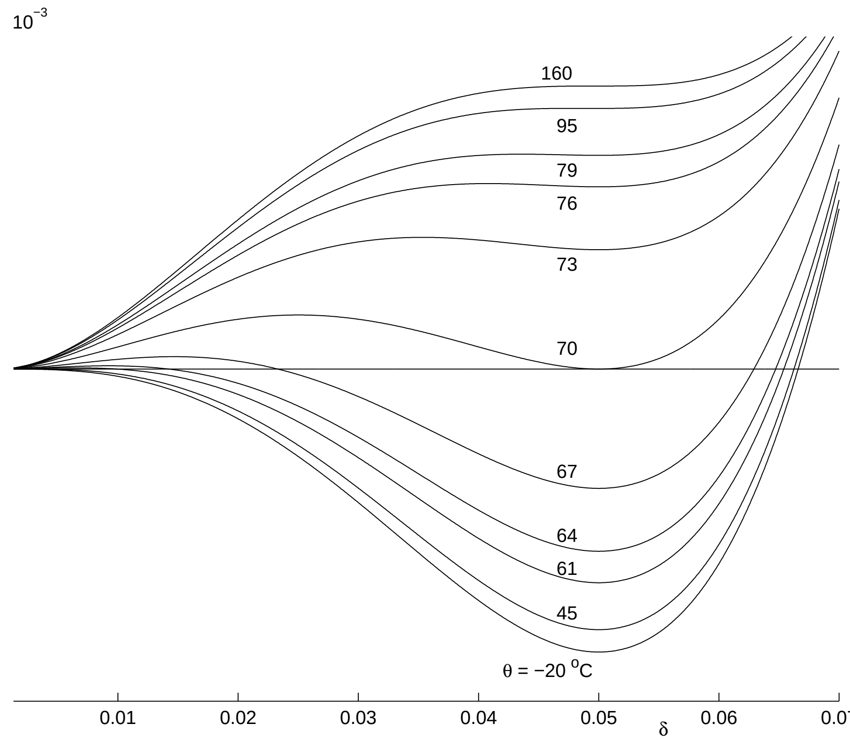

FIGURE 1. The energy density $\Phi(C_\delta,\ \theta)$ with $\theta_T = 70\,^{\circ}\mathrm{C}$.

where $\mathbf{a}^{\pm} = \sqrt{2}\varepsilon(\eta_1,\ \mp\eta_2)^T$ and $\mathbf{n}^{\pm} = \frac{1}{\sqrt{2}}(1,\ \pm 1)^T$.

It is also well known [1, 2] that, if the affine boundary condition $u(x) = A^{\pm}_{\lambda}x$, where

$$A^{\pm}_{\lambda} = (1-\lambda)U_0 + \lambda R^{\pm}U_1, \quad 0 < \lambda < 1 \tag{3.5}$$

is imposed on the boundary $\partial\Omega$, then the Young measure derived from any minimizing sequence of the elastic energy $F(u;\ \Omega)$ is unique and is given by

$$\mu^{\lambda}_{x}(\xi) \equiv \mu^{\lambda}(\xi) = (1-\lambda)\delta_{U_0}(\xi) + \lambda\delta_{R^{\pm}U_1}(\xi), \tag{3.6}$$

where δ_E is the Dirac measure centered at E, and typical minimizing sequences of $F(\cdot;\ \Omega)$ are essentially given by the finer and finer twinned layers, where the deformation gradient takes its values at U_0 and $R^{\pm}U_1$ with the volume fractions $(1-\lambda)$ and λ, modified only in a corresponding small neighbourhood of the boundary $\partial\Omega$ by a linear interpolation so that the boundary condition can be satisfied.

In our numerical examples, the initial twinned layers are taken of the following form (cf. [7, 11])

$$u^-_{\lambda,\delta}(x) = U_0 x + \delta\Big(\int_0^{\delta^{-1}x\cdot\mathbf{n}^-} \sigma_{\lambda,\delta}(s)\, ds\Big)\mathbf{a}^-, \tag{3.7}$$

where $\sigma_{\lambda,\delta}(s) = \sigma_\lambda(\delta^{-1}s)$ and

$$\sigma_\lambda(s) = \begin{cases} 0, & k \le s < k+1-\lambda, \forall k \in \mathfrak{I}, \\ 1, & k-\lambda \le s < k, \forall k \in \mathfrak{I}, \end{cases} \tag{3.8}$$

and where $\mathfrak{I}$ is the set of all integers. It is easily seen that the gradient of the deformation $u^-_{\lambda,\delta}$ takes its values at U_0 and $R^- U_1$ with the volume fractions $(1-\lambda)$ and λ and the width of a twinned layer is δ.

We can easily establish rank-one connections between the twinned martensite $A^\pm_\lambda$ and a single variant of martensite. Let

$$\theta^0_\lambda \;=\; \arctan \frac{2\lambda\varepsilon\eta_1\eta_2}{\eta_1^2\eta_2^2 - \lambda^2\varepsilon^2}, \tag{3.9}$$

$$\theta^1_\lambda \;=\; \arctan \frac{\lambda\varepsilon(1+\lambda^2\varepsilon^2)\eta_1^2\eta_2^2 - a\varepsilon}{(1+(1+a)\lambda^2\varepsilon^2)\eta_1\eta_2}, \tag{3.10}$$

where $a = 1-\lambda+\lambda\varepsilon^2$, then it is easily verified that there exist $\mathbf{a}^i_\lambda \in R^2$ and $\mathbf{n}^i_\lambda \in S^1 = \{x \in R^2 : \|x\| = 1\}$ such that

$$A^-_\lambda - R(\theta^i_\lambda)U_i = \mathbf{a}^i_\lambda \otimes \mathbf{n}^i_\lambda, \quad i = 0, 1, \tag{3.11}$$

where, in (3.11) and in the rest of the paper,

$$R(\theta) = \begin{pmatrix} \cos\theta & -\sin\theta \\ \sin\theta & \cos\theta \end{pmatrix}$$

is a rotational matrix, and we have for $\lambda \neq 1$

$$\mathbf{n}^0_\lambda \cdot \mathbf{n}^- = O(\varepsilon^2) \text{ and } \mathbf{n}^1_\lambda \cdot \mathbf{n}^- = O(\varepsilon). \tag{3.12}$$

Let $\Omega = L_0(\alpha,\beta)D$ where $D = (-a,\ a) \times (-b,\ b)$ is a $2a \times 2b$ rectangular domain, $L_0(\alpha,\beta)$ is defined by

$$L_0(\alpha,\beta)\begin{pmatrix} x \\ y \end{pmatrix} = R(\alpha)\begin{pmatrix} x + y\tan(\alpha-\beta) \\ y \end{pmatrix},$$

where $R(\alpha)$ is a rotational matrix. It is easily seen that the domain Ω so defined is a parallelogram with sides of length $2a$ and $2b\sqrt{1+\tan^2(\alpha-\beta)}$ perpendicular to $\mathbf{n}(\alpha\pm\pi/2)$ and $\mathbf{n}(\beta)$ respectively (see figure 2), where $\mathbf{n}(\tau) = (\cos(\tau), \sin(\tau))^T$. In the following examples, α is taken to be $\pi/4$ so that the laminate is parallel to the sides of length $2a$.

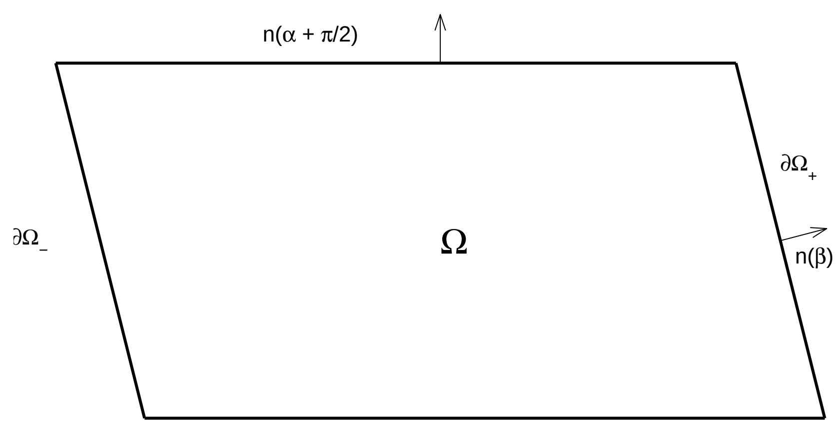

FIGURE 2. The reference configuration Ω (when $\alpha < \beta$).

To reduce the discrete error, the initial mesh should be introduced to allow the twins to bend equally easily to the either side. Naturally, in our numerical experiments, the initial mesh is introduced by $\mathfrak{T}_h(\Omega)$ which is a family of regular triangulations defined by

$$\mathfrak{T}_h(\Omega) = \mathfrak{T}_h(L_0(\alpha,\beta)D) = \{L_0(\alpha,\beta)K : \forall K \in \mathfrak{T}_h(D)\}, \tag{3.13}$$

where $\mathfrak{T}_h(D)$, for $h = h_{N,M} = \frac{2}{N\cdot M}\sqrt{(aM)^2+(bN)^2}$ with $N \geq 2$ and $M \geq 2$, is a family of regular triangulations of D introduced by the lines

$$\begin{cases} y = & -b + \frac{2b}{M}i, \qquad -M \leq i \leq M; \\ x = & -a + \frac{2a}{N}j, \qquad -N \leq j \leq N; \\ y = & \frac{b}{a}x - \frac{4b}{N}k, \qquad -\frac{N}{2} < k < \frac{N}{2}; \\ y = & \frac{-b}{a}x + \frac{4b}{N}k, \qquad -\frac{N}{2} < k < \frac{N}{2}. \end{cases} \tag{3.14}$$

Let $\partial\Omega_\pm = L_0(\alpha,\beta)\{(x,y) \in \partial D : x = \pm a\}$, and let $\partial\Omega_0 = \partial\Omega_+ \cup \partial\Omega_-$.

Numerical experiments show, as is expected, that the finer initial mesh with small random initial deformation generally leads to finer twinned layers, usually in the mesh scale. To compute needle-like microstructures with a fixed length scale, we started at a coarse mesh and refined the mesh by steps after the convergence is achieved in each step. The initial mesh should be able to accommodate the thin long needles which we expect to have, that requires $a \gg b$ if M and N is taken of the same scale. Our numerical experiments show that the needles so obtained are stable, *i.e.* they keep topologically unchanged after mesh refinements, while in the case when $a \gg b$ is not satisfied needles are often difficult to form or unstable.

Noticing the periodicity of the twinned laminate, to further relax the discrete problem, we can impose the boundary conditions in the following way (see [19]): the mesh transformation L satisfies the periodic condition

$$(L-I)(L_0(\alpha,\beta)((x,b)^T)) = (L-I)(L_0(\alpha,\beta)((x,-b)^T)), \forall x \in [-a,\ a], \quad (3.15)$$

$$L(\partial\Omega_\pm) = \partial\Omega_\pm, \quad (3.16)$$

where I is the identity map, and the deformation $\bar{u}(x) = u(L(x)) - A_\lambda^- Lx$ is also asked to satisfy the periodic condition

$$\bar{u}(L_0(\alpha,\beta)(x,b)^T) = \bar{u}(L_0(\alpha,\beta)(x,-b)^T), \quad \forall x \in [-a,\ a], \quad (3.17)$$

$$\bar{u}(x) = 0, \quad \forall x \in \partial\Omega_0. \quad (3.18)$$

The problem is thus equivalent to computing, on a domain which is infinite in the directions $\pm L_0(\alpha,\beta)(0,b)^T$, a solution which is periodic in the corresponding directions with period $2b/\cos(\alpha-\beta)$, and naturally this also allows us to focus our computation on a couple of twins so that the scale of the computation and the total cost are much reduced.

We emphasize here that our interest is to compute, under the given boundary condition, those metastable states of $F(\cdot,\ \Omega)$ which are associated to the initially existing twinned layers. In our numerical experiments, the conjugate gradient method, which is restarted at every 20 steps, was used together with a linear search to solve the discrete problem (DP) (see (2.10)), where the mesh transformation L was kept fixed until the energy gradient dropped to a certain level (for example 10^{-4}) so as to prevent the mesh from being distorted too much in the region where the gradient of the initial energy is great. To guarantee that the condition $\det \nabla L_h(x) > 0$ is satisfied, *i.e.* to keep the orientation of each element unchanged, we check the condition on each element while searching for the minimizer and reduce the step length if necessary.

To visualize the numerical results, we displayed, in the reference configuration or in the deformed configuration, an element white where the right Cauchy-Green strain tensor $C = \nabla u^T \nabla u$ is sufficiently close to $U_0^T U_0$ and black where the right Cauchy-Green strain tensor $C = \nabla u^T \nabla u$ is sufficiently close to $U_1^T U_1$, which represent the two single variants of the martensite phase, and we displayed an element gray where the right Cauchy-Green strain tensor $C = \nabla u^T \nabla u$ is neither close enough to $U_0^T U_0$ nor close enough to $U_1^T U_1$, and the darkness depends on the closeness to $U_0^T U_0$ and $U_1^T U_1$.

We consider the case for the laminate-single variant of martensite in which the deformation gradient of the boundary data is rank-one connected to the average deformation gradient of the initially given laminates as in [23], however we do not limit our computation in a thin boundary layer (compare [23]), instead we choose a physical configuration which is much longer in the direction parallel to the laminate.

Example 1. Let $\Omega = L_0(\pi/4, \alpha_{\lambda,0})D$ where $D = (-a,\ a) \times (-b,\ b)$ with $a = 3$ and $b = 0.05$, and where $\alpha_{\lambda,0}$ is the angle between the vector $\mathbf{n}_\lambda^0$ (see (3.11)) and the x axis. The initial mesh is given by $\mathfrak{T}_h(\Omega) = \mathfrak{T}_h(L_0(\pi/4, \alpha_{\lambda,0})D)$ (see (3.13) and (3.14)) with $M_0 = 16$ and $N_0 = 12$. Denote the nodes of the mesh $\mathfrak{T}_h(D)$ by

$$x_{ij} = \begin{pmatrix} -a + 2a\frac{i}{M_0} \\ -b + 2b\frac{j}{N_0} \end{pmatrix}, \quad 0 \le i \le M_0,\ 0 \le j \le N_0,$$

and denote the corresponding nodes of the mesh $\mathfrak{T}_h(\Omega)$ by $X_{ij} = L_0(\pi/4, \alpha_{\lambda,0})x_{ij}$. By (3.11), the matrix $R(\theta_\lambda^0)U_0$, which is a single variant of martensitic phase, is rank one connected to the matrix A_λ^-, which is the average of the gradients of the twinning, and the rank one direction is $\mathbf{n}_\lambda^0$. This allows us to take the initial deformation $u_{\lambda,\delta}^0(x)$ for the conjugate gradient iteration in the piece-wise linear finite element function space by setting

$$u_{\lambda,\delta}^0(X_{ij}) = \begin{cases} u_{\lambda,3\delta}^-(X_{ij}), & \text{if } i \le 3, \\ u_{\lambda,3\delta}^-(X_{ij}), & \text{else if } i \le 11 \text{ and } j \le 5, \\ u_{\lambda,\delta}^-(X_{ij}), & \text{else if } i \le 11 \text{ and } j > 5, \\ R(\theta_\lambda^0)U_0\,(X_{ij} - d), & \text{else if } 12 \le i \le 14, \\ R(\theta_\lambda^0)R^+U_1\,(X_{ij} - d), & \text{otherwise,} \end{cases} \tag{3.19}$$

where $\delta = 8b/N_0$ and $d = X_{i_0 j_0}$ with $i_0 = 14$ and $j_0 = 6$. In our numerical experiments, we take $\lambda = 0.5$, and the temperature is fixed to $55\,^{\circ}$C. The initial mesh and the distribution of the initial deformation gradient on the reference configuration $\Omega = L_0(\pi/4, \alpha_{\lambda,0})D$ are shown in Figure 3.

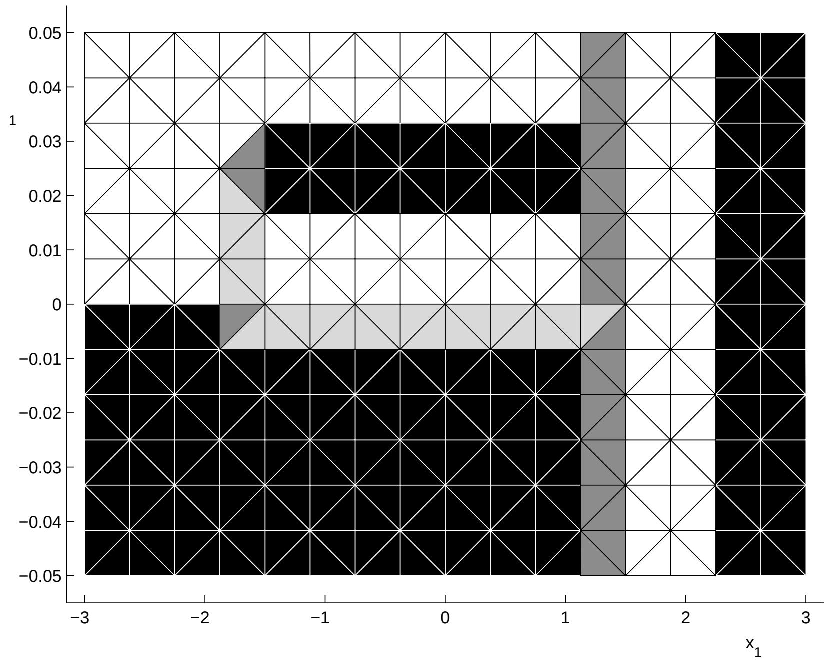

FIGURE 3. The initial mesh and deformation gradient.

To apply the mesh transformation method with periodic relaxation boundary conditions, we take

$$\bar{u}_0^0(X) = u_{\lambda,\delta}^0(X) - A_\lambda^- X, \ \forall X \in \Omega, \tag{3.20}$$

$$L_0^0(X) = I(X), \ \forall X \in \Omega, \tag{3.21}$$

as the initial deformation and mesh transformation map, and search, by the conjugate gradient method, a minimizer $(\bar{u}^0, \ L^0)$, where $(\bar{u}^0 - \bar{u}_0^0, \ L^0)$ are finite element functions in $\mathbb{U}_{h_{M_0,N_0}}(\Omega) \times \mathbb{U}_{h_{M_0,N_0}}(\Omega)$ satisfying the periodic conditions (3.15)-(3.18), of the energy functional $F(\bar{u}, L; \ \Omega)$ defined by (2.6). When the iteration is convergent, for example the energy falls no more than 10^{-12} in an iteration, then the mesh is refined by setting $M_i = 2M_{i-1}$ and $N_i = 2N_{i-1}$, $i = 1, 2, \cdots$. The pair of initial deformation and mesh transformation map $(\bar{u}_0^i, \ L_0^i)$ is taken to be the linear interpolation of $(\bar{u}^{i-1}, \ L^{i-1})$ in $\mathbb{U}_{h_{M_i,N_i}}(\Omega) \times \mathbb{U}_{h_{M_i,N_i}}(\Omega)$, where

$(\bar{u}^{i-1},\ L^{i-1})$ is the approximate minimizer obtained by the conjugate gradient method in $\mathbb{U}_{h_{M_{i-1},N_{i-1}}}(\Omega) \times \mathbb{U}_{h_{M_{i-1},N_{i-1}}}(\Omega)$ with $(\bar{u}^{i-1} - \bar{u}_0^{i-1},\ L^{i-1})$ satisfying the periodic conditions (3.15)-(3.18).

The convergence of the algorithm for the deformation and mesh transformation is shown in Table 1, where $eu_{ij}^{k,p} = \|\bar{u}^i - \bar{u}_0^i\|_{k,p}$ and $eL_{ij}^{k,p} = \|L^i - L_0^i\|_{k,p}$. The convergence of the algorithm for the energy is shown in Figure 4, where Figure 4(a) shows the convergence of the conjugate gradient method in searching for a minimizer in $\mathbb{U}_{h_{M_0,N_0}}(\Omega) \times \mathbb{U}_{h_{M_0,N_0}}(\Omega)$ and where Figure 4(b) shows the convergence of the mesh refinements combined with searching for a minimizer $(\bar{u}^i,\ L^i)$ in $\mathbb{U}_{h_{M_i,N_i}}(\Omega) \times \mathbb{U}_{h_{M_i,N_i}}(\Omega)$ by the conjugate gradient method.

TABLE 1. The convergence of the deformation and mesh transformation

$i,\ j$	$eu_{ij}^{0,2}$	$eu_{ij}^{0,\infty}$	$eu_{ij}^{1,2}$	$eL_{ij}^{0,2}$	$eL_{ij}^{0,\infty}$	$eL_{ij}^{1,2}$
0, 1	7.87×10^{-5}	7.41×10^{-4}	7.23×10^{-3}	5.51×10^{-5}	1.33×10^{-3}	3.24×10^{-2}
1, 2	2.00×10^{-5}	2.18×10^{-4}	1.94×10^{-3}	1.79×10^{-5}	7.16×10^{-4}	1.89×10^{-2}
2, 3	2.77×10^{-6}	4.79×10^{-5}	7.87×10^{-4}	1.83×10^{-6}	1.21×10^{-4}	4.50×10^{-3}
3, 4	3.38×10^{-7}	7.30×10^{-6}	3.55×10^{-4}	3.42×10^{-7}	1.21×10^{-4}	1.91×10^{-3}

Figure 5 shows the deformed mesh and the distribution of the deformation gradient on the reference configuration $L^0(L_0(\pi/4, \alpha_{\lambda,0})D)$ for the numerical result $(\bar{u}^0,\ L^0)$. In figure 6, we show on the deformed configuration the bending and branching needle-like microstructure constructed from the numerical result $(\bar{u}^3,\ L^3)$ by a periodic extension.

Example 2. Let everything be the same as in Example 1 except that the initial deformation $u_{\lambda,\delta}^0(X_{ij})$ be given by

$$u_{\lambda,\delta}^0(X_{ij}) = \begin{cases} u_{\lambda,3\delta}^-(X_{ij}), & \text{if } i \le 11, \\ R(\theta_\lambda^0)U_0\,(X_{ij} - d), & \text{else if } 12 \le i \le 14, \\ R(\theta_\lambda^0)R^+U_1\,(X_{ij} - d), & \text{otherwise}, \end{cases} \tag{3.22}$$

where $\delta = 8b/N_0$ and $d = X_{i_0 j_0}$ with $i_0 = 14$ and $j_0 = 6$. The initial mesh and the distribution of the initial deformation gradient on the reference configuration $L_0(\pi/4, \alpha_{\lambda,0})D$ are shown in Figure 7(a).

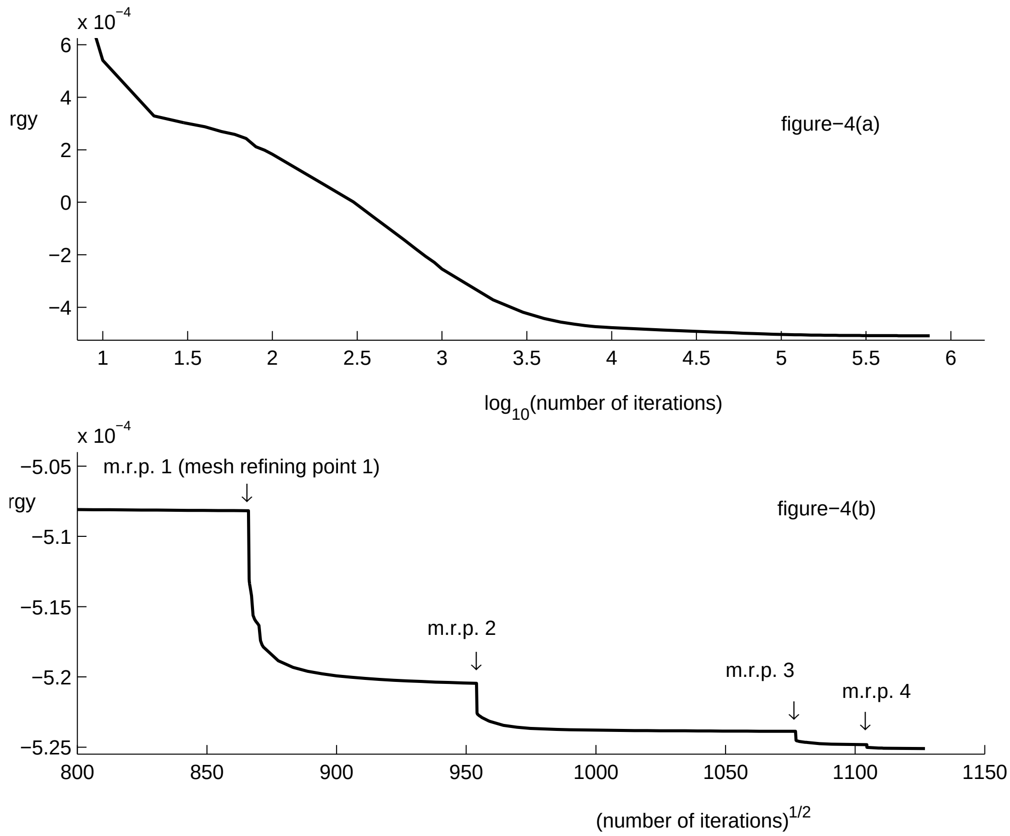

FIGURE 4. The convergence of the energy.

The numerical result of the corresponding $(\bar{u}^0, L^0)$ on the reference configuration is shown in Figure 7(b), and the corresponding bending and branching needles on the deformed configuration constructed from $(\bar{u}^3, L^3)$ by a periodic extension is shown in Figure 7(c).

Example 3. Let everything be the same as in Example 1 except that the initial deformation $u^0_{\lambda,\delta}(X_{ij})$ be given by

$$u^0_{\lambda,\delta}(X_{ij}) = \begin{cases} u^-_{\lambda,3\delta}(X_{ij}), & \text{if } i \leq 3, \\ u^-_{\lambda,\delta}(X_{ij}), & \text{else if } i \leq 11, \\ R(\theta^0_\lambda)U_0\,(X_{ij} - d), & \text{else if } 12 \leq i \leq 14, \\ R(\theta^0_\lambda)R^+U_1\,(X_{ij} - d), & \text{otherwise,} \end{cases} \tag{3.23}$$

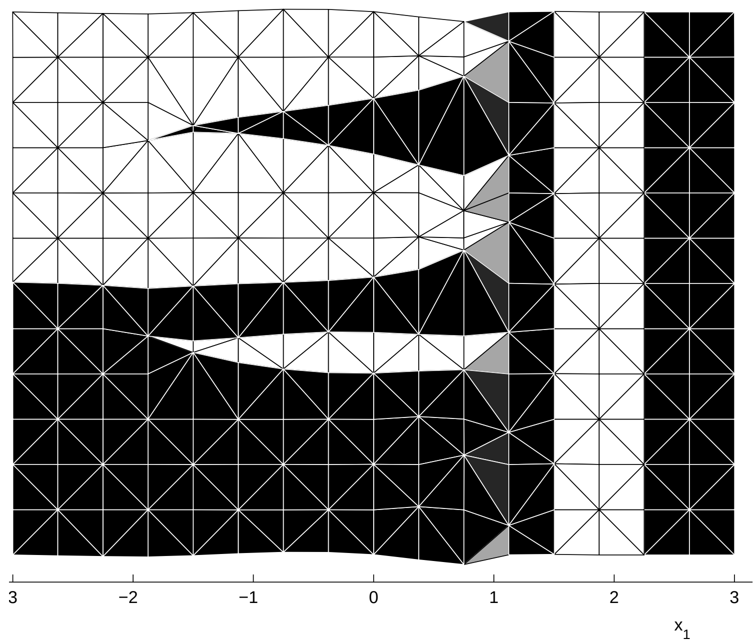

FIGURE 5. The deformed mesh and the distribution of deformation gradient for the numerical result $(\bar{u}^0,\ L^0)$.

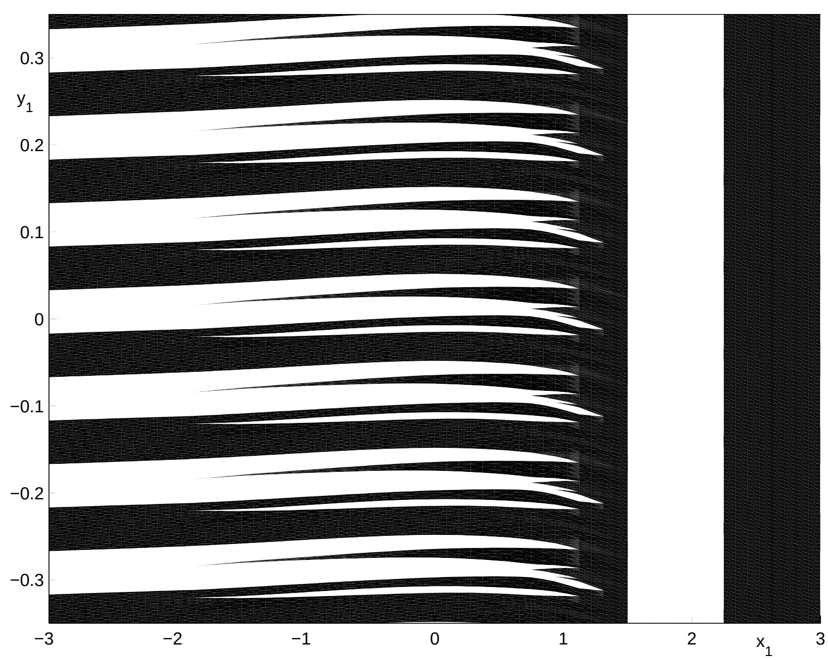

FIGURE 6. The bending and branching needles constructed from the numerical result $(\bar{u}^3,\ L^3)$.

where $\delta = 8b/N_0$ and $d = X_{i_0 j_0}$ with $i_0 = 14$ and $j_0 = 6$. The initial mesh and the distribution of the initial deformation gradient on the reference configuration $L_0(\pi/4, \alpha_{\lambda,0})D$ are shown in Figure 8(a).

The numerical result of the corresponding $(\bar{u}^0, L^0)$ on the reference configuration is shown in Figure 8(b), and the corresponding bending and branching needles on the deformed configuration constructed from $(\bar{u}^3, L^3)$ by a periodic extension is shown in Figure 8(c).

Generally, different initial data lead to different branching needles. Compare with the elastic energy of a pure variant of martensite at the temperature, that is $F(U_0; \Omega) = \Phi(C_\varepsilon, 55)\,\mathrm{meas}(\Omega) = -0.5265227 \times 10^{-3}$, we see in table 2 that the longer branched needles (figure 6 and figure 8(c)) have obviously lower interface energy $S(\bar{u}^4, L^4; \Omega) = F(\bar{u}^4, L^4; \Omega) - F(U_0; \Omega)$ than that of the needles branched only at the needle tips (figure 7(c)).

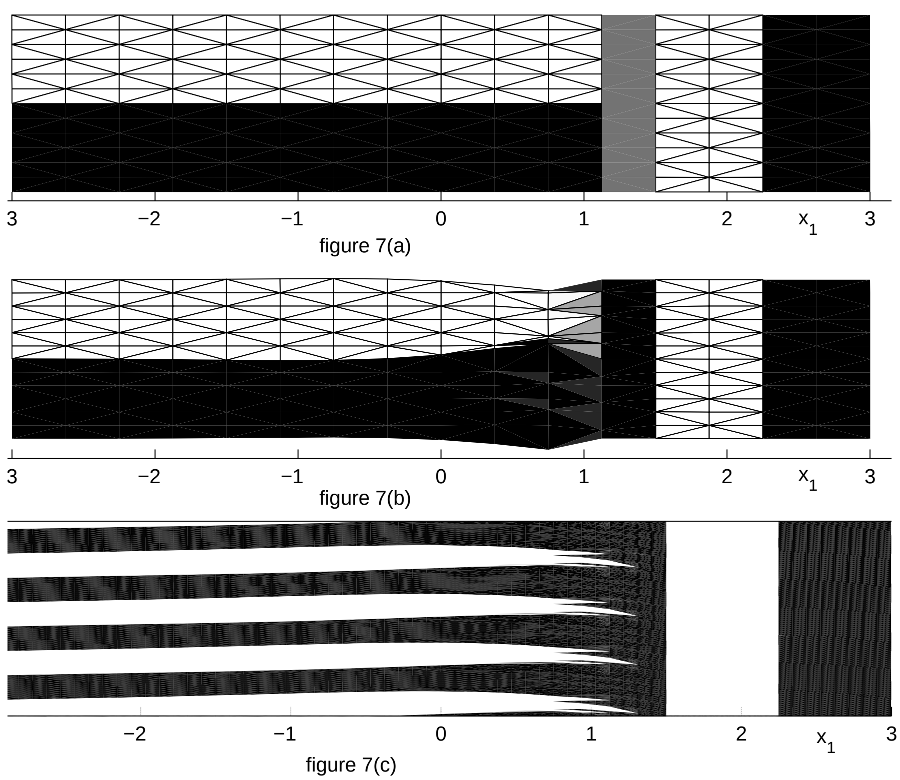

FIGURE 7. The numerical results for Example 2.

Table 2. The elastic energies for different needles

figure	6	7(c)	8(c)
$F(\bar{u}^4, L^4; \Omega)$	$-0.5250724 \times 10^{-3}$	$-0.5242411 \times 10^{-3}$	$-0.5249441 \times 10^{-3}$
$S(\bar{u}^4, L^4; \Omega)$	0.1450849×10^{-5}	0.2281639×10^{-5}	0.1578589×10^{-5}

References

[1] J. M. Ball and R. D. James, *Fine phase mixtures as minimizers of energy.* **Arch. Rat. Mech. Anal., 100**(1987)1, 13-52.

[2] J. M. Ball and R. D. James, *Proposed experimental test of a theory of fine microstructure and the two-well problem.* **Phil. Trans. R. Soc. London 338A**(1992), 389-450.

[3] J.M. Ball, *A version of the fundamental theorem for Young measures.* In **Partial Differential Equations and Continuum models of Phase Transitions**, Lecture Notes in Physics, No. 344, M. Rascle, D. Serre and M. Slemrod, eds., Springer-Verlag, New York (1989), pp. 207-215.

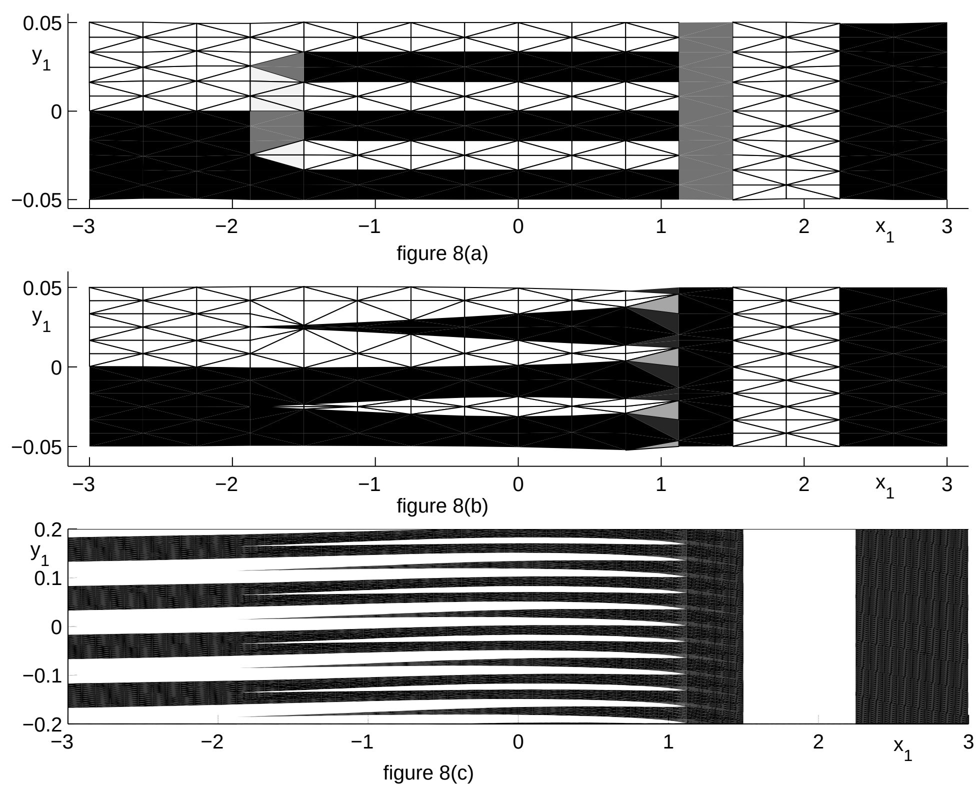

Figure 8. The numerical results for Example 3.

[4] C. Collins and M Luskin, *The computation of the austenitic-martensitic phase transition.* In **Partial Differential Equations and Continuum Models of Phase Transitions** Lecture Nodes in Physics, Vol. 344, M. Rascle, D. Serre and M. Slemrod, eds, Springer-Verlag, New York, (1989), pp. 34-50.

[5] M. Chipot, *Numerical analysis of oscillations in nonconvex problems.* **Numer. Math., 59**(1991), 747-767.

[6] C. Collins, *Computation of twinning*, in **Microstructure and Phase Transitions**, IMA Volumes in Mathematics and Its Applications, Vol.54, J. Ericksen, R. James, D. Kinderlehrer and M. Luskin, eds, Springer-Verlag, New York, (1993), pp. 39-50.

[7] C. Collins, M. Luskin and J. Riordan, *Computational results for a two-dimensional model of crystalline microstructure*, in **Microstructure and Phase Transitions**, IMA Volumes in Mathematics and Its Applications, Vol.54, J. Ericksen, R. James, D. Kinderlehrer and M. Luskin, eds, Springer-Verlag, New York, (1993), pp. 51-56.

[8] M. Chipot, C. Collins and D. Kinderlehrer, *Numerical analysis of oscillations in multiple well problems.* **Numer. Math., 70**(1995), 259-282.

[9] P. Gremaud, *Numerical optimization and quasiconvexity*, **Euro. J. Appl. Math., 6**(1995) 69-82.

[10] P. Pedregal, *On the numerical analysis of non-convex variational problems*, **Numer. Math., 74**(1996), 325-336.

[11] M. Luskin, *On the computation of crystalline microstructure.* **Acta Numerica, 5**(1996), 191-257.

[12] R. A. Nicolaides, N. Walkington and H. Wang, *Numerical methods for a nonconvex optimization problem modeling martensitic microstructure.* **SIAM J. Sci. Comput., 18**(1997), 1122-1141.

[13] Z.-P. Li, *Simultaneous numerical approximation of microstructures and relaxed minimizers.* **Numer. Math., 78** (1997), 21-38.

[14] Z.-P. Li, *Laminated microstructure in a variational problem with a non-rank-one connected double well potential*, **J. Math. Anal. Appl., 217**(1998), 490-500.

[15] Z.-P. Li, *Rotational transformation method and some numerical techniques for the computation of microstructures.* **Math. Models Meth. Appl. Sci., 8**(1998), 985-1002.

[16] C. R. Collins, *Convergence of a reduced integration method for computing microstructures.* **SIAM J. Numer. Anal., 35**(1998), 1271-1298.

[17] M.K. Gobbert and A. Prohl, *A discontinuous finite element method for solving a multi-well problem.* IMA preprint series #1539, University of Minnesota.

[18] Z.-P. Li, *A mesh transformation method for computing microstructures.* To appear in **Numer. Math.**.

[19] Z.-P. Li, *A periodic relaxation method for computing microstructures.* **Appl. Numer. Math., 32**(2000), 291-303.

[20] Z. -P. Li, *A coupled numerical method for relaxed minimizers and inhomogeneous microstructures*. In **Proceedings of 4th International Conference/Exhibition on High Performance Computing in Asia-Pacific Region**, Volume II, IEEE Computer Society, (2000), pp. 1022-1024.

[21] Z.-P. Li, *Finite order rank-one convex envelopes and computation of microstructures with laminates in laminates*. To appear in **BIT Numer. Math.**.

[22] M. G. Killough, *A diffuse interface approach to the development of microstructure in martensite*, Ph.D. thesis, New York University, 1998.

[23] B. Li and M. Luskin, *Theory and computation for the microstructure near the interface between twinned layers and a pure variant of martensite*. To appear in **Materials Sci. Eng. A**.

[24] R. Abeyaratne, C. Chu and R. D. James, *Kinetics of materials with wiggly energies: the evolution of twinning microstructure in a Cu-Al-Ni shape memory alloy*. **Phil. Mag. 73A** (1996), 457-497.

[25] R.D. James, R.V. Kohn and T.W. Shield, *Modeling the branched needle microstructures at the edge of a martensite laminate*, ICOMAT-95, **J. de Physique IV**, 5(1995), 253-259.

[26] B. Li, *Analysis and computation of martensitic microstructure*, Ph.D. thesis, University of Minnesota, 1996.

[27] C.-H. Chu, *Hysteresis and microstructures: a study of biaxial loading on compound twins of Copper-Aluminum-Nickel single crystals*, Ph.D. Thesis, University of Minnesota, 1993.

[28] R.V. Kohn and S. Müller, *Branching of twins near an austenite-twinned martensite interface*. **Phil. Mag., 66A**(1992), 697-715.

[29] Z.-P. Li, *Mesh re-regularization and quasi-static numerical simulation of austenitic-martensitic phase transition*. Research Report No.11, Institute of Mathematics and School of Mathematical Sciences, Peking University, 2000.

[30] P. Klouček and M. Luskin, *The computation of the dynamics of the martensitic transformation*, *Continuum Mech. Thermodyn., 6*(1994), 209-240.

[31] P.G. Ciarlet, **The Finite Element Method for Elliptic Problems**. North-Holland, Amsterdam, 1978.

[32] R.A. Adams, **The Sobolev Spaces**. Academic Press, New York, 1975.